Acta Biomaterialia 73 (2018) 141–153

Contents lists available at ScienceDirect

Acta Biomaterialia

journal homepage: www.elsevier.com/locate/actabiomat

Full length article

Exploring the potential of polyurethane-based soft foam as cell-free scaffold for soft tissue regeneration

Irini Gerges [a,b,*,1], Margherita Tamplenizza [a,b,1], Federico Martello [a,b], Camilla Recordati [b], Cristina Martelli [c], Luisa Ottobrini [c,d], Mariacaterina Tamplenizza [a], Scott A. Guelcher [e], Alessandro Tocchio [a,f], Cristina Lenardi [b,g]

[a] Tensive S.r.l., Via Timavo 34, 20124 Milan, Italy
[b] Fondazione Filarete, Viale Ortles 22/4, 20139 Milan, Italy
[c] Department of Pathophysiology and Transplantation, University of Milan, Via Fratelli Cervi 93, 20090 Segrate, Italy
[d] Institute for Molecular Bioimaging and Physiology (IBFM), National Research Council (CNR), Milan, Italy
[e] Department of Chemical and Biomolecular Engineering, Vanderbilt University, PMB 351604 2301 Vanderbilt Place, Nashville, TN 37235-1604, USA
[f] SEMM, European School of Molecular Medicine, Campus IFOM-IEO, Via Adamello 16, 20139 Milano, Italy
[g] CIMAINA, Dipartimento di Fisica, Università degli Studi di Milano, Via Celoria 16, 20133 Milan, Italy

ARTICLE INFO

Article history:
Received 27 November 2017
Received in revised form 23 March 2018
Accepted 4 April 2018
Available online 12 April 2018

Keywords:
Soft tissue regeneration
Poly(urethane-ester-ether)
Adipose tissue
Vascularization
Breast reconstruction

ABSTRACT

Reconstructive treatment after trauma and tumor resection would greatly benefit from an effective soft tissue regeneration. The use of cell-free scaffolds for adipose tissue regeneration *in vivo* is emerging as an attractive alternative to tissue-engineered constructs, since this approach avoids complications due to cell manipulation and lack of synchronous vascularization. In this study, we developed a biodegradable polyurethane-based scaffold for soft tissue regeneration, characterized by an exceptional combination between softness and resilience. Exploring the potential as a cell-free scaffold required profound understanding of the impact of its intrinsic physico-chemical properties on the biological performance *in vivo*. We investigated the effect of the scaffold's hydrophilic character, degradation kinetics, and internal morphology on *(i)* the local inflammatory response and activation of MGCs (foreign body response); *(ii)* its ability to promote rapid vascularisation, cell infiltration and migration through the scaffold over time; and *(iii)* the grade of maturation of the newly formed tissue into vascularized soft tissue in a murine model. The study revealed that soft tissue regeneration *in vivo* proceeded by gradual infiltration of undifferentiated mesenchymal cells though the periphery toward the center of the scaffold, where the rapid formation of a functional and well-formed vascular network supported cell viability overtime.

Statement of significance

Exploring the potential of polyurethane-based soft foam as cell-free scaffold for soft tissue regeneration.

In this work, we address the unmet need for synthetic functional soft tissue substitutes that provide adequate biological and mechanical support to soft tissue. We developed a series of flexible cross-linked polyurethane copolymer scaffolds with remarkable fatigue-resistance and tunable physico-chemical properties for soft tissue regeneration *in vivo*. Accordingly, we could extend the potential of this class of biomaterials, which was so far confined for bone and osteochondral tissue regeneration, to other types of connective tissue.

1. Introduction

Adipose tissue regeneration aims to restore portions of damaged tissue after trauma and tumor resection. Earlier surgical approaches based on autologous fat grafting have shown limited success for restoration of small adipose tissue defects due to volume loss and the lack of neovascularization of the grafted tissue

* Corresponding author at: Tensive S.r.l., Via Timavo 34, 20124 Milan, Italy.
E-mail address: irini.gerges@tensivemed.com (I. Gerges).
[1] Authors IG and MT contributed equally to this work.

https://doi.org/10.1016/j.actbio.2018.04.011
1742-7061/

[1]. The employment of naturally derived soft matrices (such as hyaluronic acid, collagen or fibrin) for the regeneration of small volumes (0.5–2 mL) of soft tissue *in vivo* is a widely used esthetic surgical practice [2]. However, the rapid enzymatic and hydrolytic degradation of such natural matrixes precludes their employment as cell-free 3D scaffolds for the regeneration of larger volumes of soft tissue *in vivo*, since they cannot guarantee adequate mechanical support during the regeneration process, which depends on the volume of tissue to be regenerated and patient-specific factors such as health and age. Cell-free scaffolds capable of stimulating adipose tissue regeneration *in vivo* are being considered as a potentially more attractive solution since they avoid costs related to cell manipulation *in vitro* [3] and simplify the regulatory approval and validation process [4]. The employment of synthetic polymers in the fabrication of functional 3D matrices is a steadily growing trend in regenerative medicine, especially for bone and cartilage repair, due to their cost-effectiveness, high reproducibility, and the ability to finely tune their properties to match those of the target tissue. Nevertheless, fabrication of scaffolds for soft tissue repair presents significant challenges due to the need to promote rapid vascularization and stimulate cell signaling pathways that promote regeneration [5]. The impact of specific physico-chemical properties on the biological performance *in vivo* is still unclear for many synthetic soft tissue scaffolds. Significant efforts have been paid to develop biodegradable synthetic biomaterials for tissue regeneration, among which crosslinked poly(glycerol sebacate), fabricated as three-dimensional porous constructs, by salt leaching technique.Current attempts aiming to develop soft scaffolds from synthetic polymers are mainly focused on the family of biodegradable linear thermoplastics, such as poly L-lactic acid (PLA) [6], poly(lactic-*co*-glycolic acid) (PLGA), poly(hydroxy butyrate) (PHB) [7], Poly(1,8-octanediol-*co*-citric acid) (POC) [8] and poly(epsilon-caprolactone) (PCL) [9]. Significant efforts have been also paid to develop biodegradable flexible and elastomeric synthetic constructs, for soft tissue regeneration, among which crosslinked poly(glycerol sebacate)-based biomaterials [10]. The mechanical properties of this class of biomaterials can be modulated by choosing an appropriate micro-fabrication technique (i.e. salt leaching, electrospinning, mesh deposition, etc.) [11]. Further investigations demonstrated that the so obtained scaffolds were suitable for soft tissue regeneration, in particular for cartilage repair [12]. The degradation products from these poly(α-esters) are converted *in vivo* to metabolites (such as lactic and glycolic acid) that are eliminated from the body by natural pathways [13]. The employment of linear polyesters in soft scaffolds fabrication require chemical modifications to improve their mechanical properties, including low stiffness and resilience (i.e. the capability to regain the original shape after deformation). Previous attempts to improve the mechanical properties of semi-crystalline biodegradable polyesters through copolymerization with hard polyurethane segments (DegraPol®) paved the way for fast expansion of polyester-based biomaterials in regenerative medicine, but still not suitable for soft tissue regeneration [14].

In this work, we address the unmet need for synthetic functional soft tissue substitutes that provide adequate biological and mechanical support to soft tissue, especially in the early stages when the extracellular matrix is not mature enough to support tissue ingrowth. We developed a series of flexible cross-linked polyurethane copolymer scaffolds with remarkable fatigue-resistance and tunable physico-chemical properties for soft tissue regeneration *in vivo*.

To evaluate the potential of polyurethane-based soft foam (soft PUF) as cell-free scaffolds, we investigated how specific physico-chemical properties (such as water-uptake capacity and degradation kinetics) impact on the local biological performance of the biomaterial *in vivo* as well as the mechanism by which soft tissue regeneration takes place throughout the scaffold. Results reported in this study demonstrated that the physico-chemical properties of these scaffolds can be tuned to targeted properties by varying the ratio of hydrophilic poly(ethylene glycol) (PEG6K) and hydrophobic polyester (PE-diol-13 K) segments in the polymeric network. *In vivo* studies, carried out by subcutaneous implantation in a murine model at multiple time points for up to 91 days, shows that soft PUFs were well tolerated *in vivo*, allowed for rapid cellular infiltration, and promoted rapid recruitment of vascular tissue. Local inflammation, Neutrophil Myeloperoxidase MPO activity, and tissue density were evaluated by *in vivo* imaging [15]. Histological analyses were carried out using hematoxylin and eosin and immunohistochemical staining. Total collagen deposition within the scaffolds was evaluated at 3 months post-implantation by Picrosirius red staining. The foreign body response was evaluated by cross-correlating data obtained from histological analysis and *in vivo* imaging.

2. Materials and methods

2.1. Materials

Glycerol 95%, xylitol 99%, glycolide 99%, ε-caprolactone 97%, poly(ethylene glycol) molecular weight 570–630 (PEG600), poly (ethylene glycol) molecular weight 6000 (PEG6K), hexamethylene diisocyanate 98% (HMDI), N,N,N′,N′-Tetramethylethylenediamine 99% (TEMED), dibutyltin dilaurate 95% (DBT), Tin(II) 2-ethylhexanoate 95%, hydroxyapatite ≥90% ($Ca_3(PO_4)_3OH$, synthetic origin, solid powder, melting point 1100° C, relative density 3.14 g/m^3) (HA), N,N-dimethylformamide ≥99.8% (DMF) and chloroform ≥99.9% were purchased from Sigma-Aldrich and used without further purification unless otherwise indicated.

2.2. Syntheses

2.2.1. Synthesis of poly(ε-caprolactone-co-glycolide)-b-poly(ethylene glycol)-b-poly(ε-caprolactone-co-glycolide)-diol (PE-diol-13 K)

PEG600 was dehydrated under reduced pressure of 0.1 mbar at room temperature (25 °C) for 48 h prior to use. 4.8 g PEG600, 62.1 mL ε-caprolactone (ρ = 1.03 g/mL, 560.7 mM) and 16.0 g glycolide (137.8 mM) were introduced in a round bottomed two-necked flask, equipped with magnetic stirrer and nitrogen inlet. The temperature of the system was raised to 80 °C and dried under reduced vacuum of 0.1 mbar for an hour before introducing 72 μL tin(II) 2-ethylhexanoate (ρ = 1.25 g/mL, 0.2 mM). The system was then deoxygenated carrying out 4 nitrogen-vacuum cycles. The reaction proceeded for 24 h at 150 °C in inert atmosphere.

The polymer was obtained as a viscous yellowish liquid (at room temperature 25 °C) and used as obtained without purification. Average molecular weights calculated from SEC (PS standards) were Mn = 13,000, Mw = 13,500, and P.D index = 1.03. ^{1}HNMR ($CDCl_3$, 400 MHz): δ = 1.39 (—O—$(CH_2)_2$—**CH_2**—$(CH_2)_2$—COO—); 1.66 (—**CH_2**—CH_2—O—C=O); 2.32–2.45 (—**CH_2**—COO—); 3.66 (—CH_2—**CH_2**—O); 4.07–4.31 (—**CH_2**—O—C=O); 4.65 (—O—**CH_2**—C=O).

The average number molecular weight Mn calculated semi-quantitatively from ^{1}HNMR ($CDCl_3$, 400 MHz) was 13,500. The hydroxyl number of the polyester: PE-diol-13 K, determined according to ASTM D4272-99 standard, was 8.6 mg KOH/g.

2.2.2. Synthesis of hydroxyapatite-filled soft PUFs with different PEG/PE ratios

In a 250 mL polypropylene beaker, equipped with mechanical stirring, 3.3 g glycerol (19.53 mM), PE-diol-13 K and/or PEG6K were introduced and dissolved in 21.6 mL DMF (ρ = 0.94 g/mL) at

70 °C under mechanical stirring at 200 rpm for 10 min. 10.0 g HA was added to the solution under mechanical stirring at 300 rpm to prepare a homogeneous paste. 10.5 g HMDI (62.78 mM) and 3.3 g aqueous solution of xylitol (50% w/w, 10.84 mM) were added at the same stirring speed and temperature. Finally, 100 μL TEMED (ρ = 0.77 g/mL) and 100 μL DBT (ρ = 1.06 g/mL) were added. Foam expansion proceeded for 20 s until the polymers reached gel-point due to cross-linking. After solidification, the row foams were kept in oven at 60 °C for 24 h to complete the reactions conversion. Cylindrical samples were then cut from the foam by means of metallic puncture and purified by continuous extraction from chloroform. Samples were dried from chloroform at 0.01 mbar for 5 days at 70 °C and stored in a dry and dark place at 4 °C. The formulations data (i.e. NCO index, the amount of: polyol components (pphp), catalysts (pphp), HA filler (% w/w) and the density of the free-rise foams (kg/m^3)) are summarized in Table 1.

A hydroxyapatite-free control formulation, named: PUF 3/10-zero HA, was synthesized according the same procedure and reactants used for PUF 3/10, except for the addition of HA filler. This formulation was used to verify the impact of HA filler on the morphological properties of the 4 PUF formulations (Table 2).

The cytotoxicity of the soft PUFs was assessed *in vitro*. Briefly, two samples were cut into three pieces and each piece was placed onto a 24-well plate. NIH 3 T3 murine fibroblast cells were seeded into each well (10,000 cells/cm^2) and the scaffold pieces completely submerged in the media. Empty well plates (no scaffold) were tested as controls (n = 3). Cell viability was monitored for 7 days. If the cells in direct contact with the scaffold had a qualitatively comparable morphology and viability to the control wells, the entire batch was released for biological experiments.

2.3. Chemico-physical characterizations

2.3.1. Morphological characterization by scanning electron microscopy (SEM)

Samples were sputter-coated with gold (Polaron E5100 Sputter Coater, Bad Schwalbach, Germany) and images acquired using a Carl ZEISS-Sigma scanning electron microscope equipped with EDS Brucker-X Flash 5030-127 eV detector.

2.3.2. Morphological characterization by μCT 3D scan

The samples were measured with a commercially available cabinet cone-beam μCT (μCT 50, SCANCO Medical AG, Brüttisellen, Switzerland) originating from a 4 μm focal-spot X-ray tube. The photons are detected by a CCD- based area detector and the projection data are computer-reconstructed into a 3072 × 3072 image matrix. The scan image was segmented with a first threshold for polymeric material with x-ray absorption >0.2 [1/cm] (equivalent −120 mgHA/ccm) and the inorganic filler particles as absorption >1.75 [1/cm] (700 mgHA/ccm). Both objects were superimposed, and 3D rendering were produced. The density distribution histogram of the scaffolds was obtained by binning all its voxels by density (excluding zeros). All image processing was carried out using IPL (Scanco Medical AG).

2.3.3. Size exclusion chromatography (SEC)

The average molecular weight of the biodegradable segment: PE-diol-13 K was determined by SEC analysis, using a chromatograph composed of Knauer isocratic pump, operating on a flow of 1.0 mL/min and THF mobile phase, 2 columns in series maintained at 35 °C: Resipor-PL (400,000–500 Da) and Tosoh (20,000–500 Da) and multidetector (Light Scattering (LS) at 7° and 90°, refractive index (RI) and Viscotek differential viscometer (VD)). The calculation of molecular weights with absolute method has been obtained with a calibration polystyrene standard solution with molecular weight of 72,000 and using Omnisec software (Viscotek).

2.3.4. In vitro swelling tests

Swelling tests were carried out in PBS 1X at 37 °C using 6 dried cylindrical samples of 8 mm diameter and 3 mm height. At each time point, namely: 1, 2, 4, 7, 24 and 48 h, the swollen samples were gently extracted from the swollen media and weighted. The swelling degree was calculated according to equation (1).

$$\text{Swelling degree } \% = (W_S - W_0) \times 100/W_0 \quad (1)$$

where W_0 and W_s are the initial and the swollen weight, respectively.

Table 1
PUF formulations data.

Formulations data	PUF 13/0	PUF 10/3	PUF 3/10	PUF 0/13
Isocyanate index (-eq. NCO*100/-eq. OH)	77.7	77.9	78.5	79.0
PEG6K (pphp*)	72.7	56.2	16.5	0.0
PE-diol-13 K (pphp)	0.0	16.5	56.2	72.7
Glycerol (pphp)	18.2	18.2	18.2	18.2
Xylitol (pphp)	9.1	9.1	9.1	9.1
Water (pphp)	9.1	9.1	9.1	9.1
TEMED (pphp)	0.4	0.4	0.4	0.4
DBT (pphp)	0.6	0.6	0.6	0.6
HA (% w/w)	25.7	25.7	25.7	25.7
Density of free-rise foam (kg/m^3)	130.0	140.0	140.0	125.0

* pphp: Based on 100 parts polyol having functionality ≥2, by weight (excluding water).

Table 2
The morphological properties of PUF formulations, obtained by μCT 3D scan, and compared to the HA-free control formulation: PUF 3/10-zero HA.

Morphological property	PUF 13/0	PUF 10/3	PUF 3/10	PUF 0/13	PUF 3/10-zero HA
Average pore diameter (mm)	0.29 (±0.14)	0.42 (±0.14)	0.29 (±0.22)	0.34 (±0.13)	0.5733 (±0.15)
Local thickness (mm)	0.04 (±0.02)	0.07 (±0.04)	0.02 (±0.01)	0.04 (±0.02)	0.06 (±0.01)
Specific surface area (m^2/m^3)	9464.58	7251.24	15607.49	7586.71	4994.23
Porosity (%)	87.01	85.79	85.27	88.36	88.65
HA filler density in the polymeric matrix (mg HA/ccm)	541.85	434.24	510.69	598.84	0.00

2.3.5. Degradation kinetics in physiological and accelerated conditions

Degradation tests were carried out at 37 °C in PBS 1X, 3% w/w H_2O_2 (ISO10993-13; 1998), or 2 M HCl. Six cylindrical samples of 8 mm diameter and 3 mm height and average dry weight 30–35 mg were tested. At each time point, samples were removed from the degradation medium, washed twice in distilled water (20 min each), then washed in ethanol for 20 min, and dried under reduced pressure (0.01 mbar) for 1 weeks. Weight loss was calculated according to equation (2).

$$\text{Weight loss } \% = (W_0 - W_d) \times 100/W_0 \quad (2)$$

where W_0 and W_d are the initial and the degraded weight at certain time point, respectively.

2.3.6. Compression tests

Mechanical properties under compression were measured using a testing machine equipped with a 100 N load cell (model BR EMT503 A, MP Strumenti, Pioltello (MI), Italy) and operated at a crosshead speed of 1 mm/min. Cylindrical samples of 8 mm diameter and 6 mm height were analyzed according to the ISO 604-1993 standard. The compressive modulus (Ec) was calculated from the slope of the stress-strain curve in the elastic region (*i.e.*, 5 to 10% strain). The yield point was determined from the stress-strain curve as the inflection point between the elastic and plastic deformation. The compressive stress was calculated at 90% strain. Measurements were carried out at room temperature (25 °C) using cylindrical samples incubated in PBS 1X for 24 h at 37 °C. Six replicates were analyzed for each test to calculate the standard deviation.

The resilience of the 4 soft PUF formulations was determined by compressing the scaffolds for 100 cycles. Each cycle consisted of compressive deformation up to 20% maximum strain (speed 1 mm/min) followed by relaxation of the stress (speed 1 mm/min) to allow the platen to reach its initial position. The measured stress (kPa) was plotted versus the number of cycles.

2.4. In vivo tests

2.4.1. Biocompatibility test

The experiment was performed in accordance with the Italian Laws (D.l.vo 116/92 and following additions) in compliance with EU 86/609 Directive (Council Directive 86/609/EEC of November 24, 1986, on the approximation of laws, regulations, and administrative provisions of the member states regarding the protection of animals used for experimental and other scientific purposes). Female CD1 mice (Charles River laboratories) aged 8 weeks (weight 25–31 g) were used for this study.

Animals were supplied with gentamicin water added (40 mg/mL) for 2 days before surgery and for further 4 days after surgery. Mice were anaesthetized by a tiletamine (40 mg/mL) and zolazepam/xylazine mixture (8 mg/kg) (Zoletil 100, Virbac) intraperitoneally. The back was epilated, disinfected and a mid 5 mm-long incision was made. Two lateral pockets were prepared from the dorsal incision. Pre-hydrated scaffolds (8 mm diameter × 4 mm height) were introduced subcutaneously in the lateral pockets. The skin was then sutured (Ethilon 6/0) and the mice allowed to recover. Mice were sacrificed at 7, 28, 48 and 91 days post-implantation (5 animals with 4 implants for each time point).

2.4.2. In vivo inflammation and CT evaluation

In vivo imaging was performed with an IVIS Spectrum/CT (PerkinElmer; kindly supplied to the IMAGO lab by IRCCS Cà Granda Foundation) at 2, 7, 28 and 48 days, after implantation [15].

The μCT scans were performed to visualize scaffold position and to evaluate absorption coefficient and Hounsfield Units of the scaffolds. Data were quantified in a 3D Region of Interest (ROI) in the scaffold including region and were expressed as Average Value for absorption coefficient (Total Value/Number of voxels in the 3D ROI) and Average Hounsfield Units (Total Hounsfield unit value/Number of voxels in the 3D ROI). Implanted mice underwent X-ray imaging to evaluate changes in the absorption coefficient and Hounsfield unit over time. The X-ray absorption coefficient represents a measurement of the amount of X-rays absorbed by the tissue voxels, whereas Hounsfield units measure the tissue radio density as graphically reported in the grayscale.

To evaluate inflammation, a 200 mg/kg XenoLight RediJect inflammation probe (PerkinElmer Inc.), a chemi-luminescent reagent for monitoring inflammation by studying Neutrophil Myeloperoxidase (MPO) activity of activated phagocytes (neutrophils and macrophages) present in the inflammatory site, was intraperitoneally administered. When injected, the probe is not chemi-luminescent by itself, but after activation of MPO a luminescence signal can be detectable. Ten minutes post-injection, bioluminescence was imaged for 5 min. Furthermore, fluorescent emission at 745/800 nm was recorded to check the accuracy of injection. Luminescence signals were quantified in each ROI and data expressed as average radiance (photons/second/cm^2/steradian).

2.4.3. Histological examination

After sacrifice, scaffolds together with the surrounding tissues were excised and fixed in 10% neutral buffered formalin. Formalin-fixed samples were embedded in paraffin wax, sectioned at 4 μm thickness, routinely stained with hematoxylin and eosin (HE), and evaluated under a light microscope for the histological assessment of host reaction (fibrous encapsulation, extent and type of inflammatory cells, necrosis, nature and extent of tissue ingrowth into the pores, cell adhesion to the material, and cell infiltration into the material) according to the ISO 10993–6 standard for biological evaluation of medical devices. The standard was slightly modified to adapt to the present studies (Supplemental data – Tables S1 and S2).

For the evaluation of the total collagen deposition within the scaffolds at day 91 post-implantation, 4-μm sections from each sample were stained with Picrosirius red and digitally photographed at x12.5 magnification. The % area of collagen (stained in red) was quantified using the ImageJ analysis program v1.49 (http://rsb.info.nih.gov/ij/) selecting as Region of Interest (ROI) the area occupied by the implanted scaffold.

2.4.4. Immunohistochemical staining

To evaluate neovascularization, scaffold sections were immunostained for CD31. Sections were deparaffinized and underwent heat-induced epitope retrieval (Dewax and HIER Buffer H, Thermo Scientific, UK). Endogenous peroxidase activity was blocked by incubating sections in 3% H_2O_2 for 15 min. Slides were rinsed and treated with PBS containing 10% normal rabbit serum for 30 min to reduce nonspecific background staining and then incubated for 1 h at room temperature with a rat monoclonal anti-CD31 antibody (Dianova, clone SZ31). Biotinylated rabbit anti-rat secondary antibody (Vector Laboratories, Burlingame, CA, USA) was then added for 30 min. Sections were labelled by the avidin–biotin-peroxidase (ABC) procedure with a commercial immunoperoxidase kit (Vectastain Standard Elite, Vector Laboratories, Burlingame, CA, USA). The immunoreaction was observed with 3,3′-diaminobenzidine substrate (DAB, Vector Laboratories, Burlingame, CA, USA) for 10 min and sections were counterstained for 2 min with Mayer's hematoxylin. Known positive control sections were included in each immunolabeling assay.

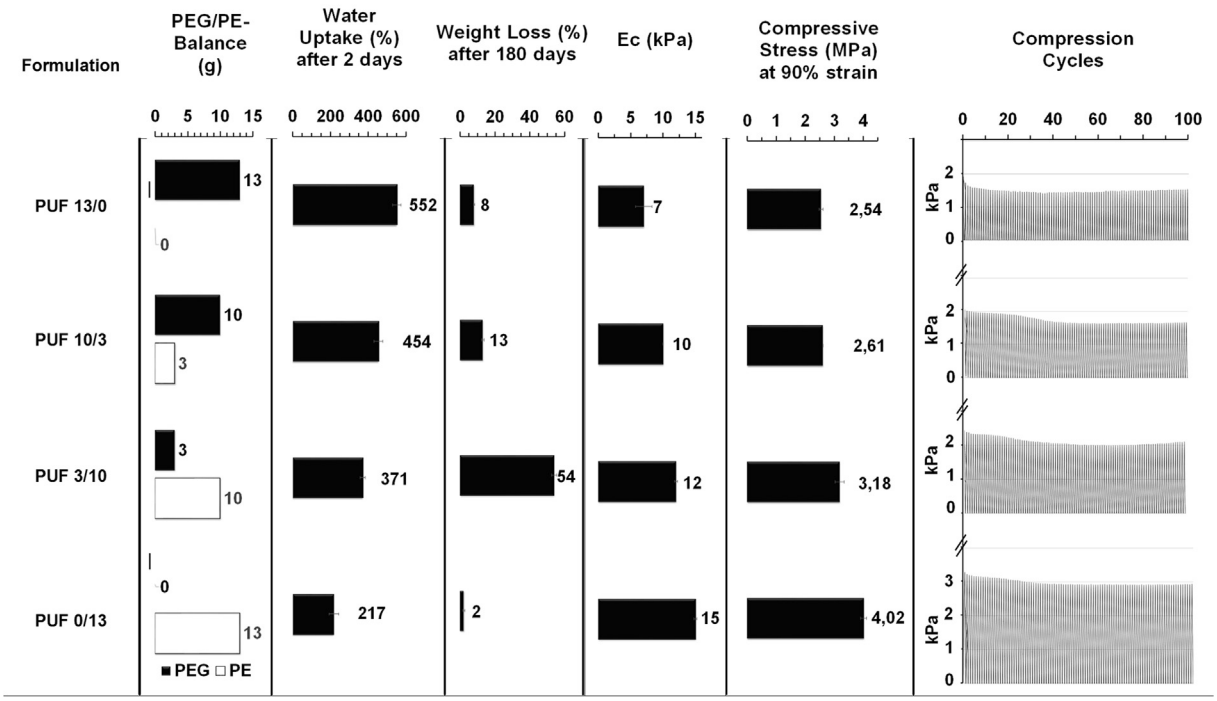

Fig. 1. Schematic representation of the physico-chemical and morphological properties of soft PUF formulations.

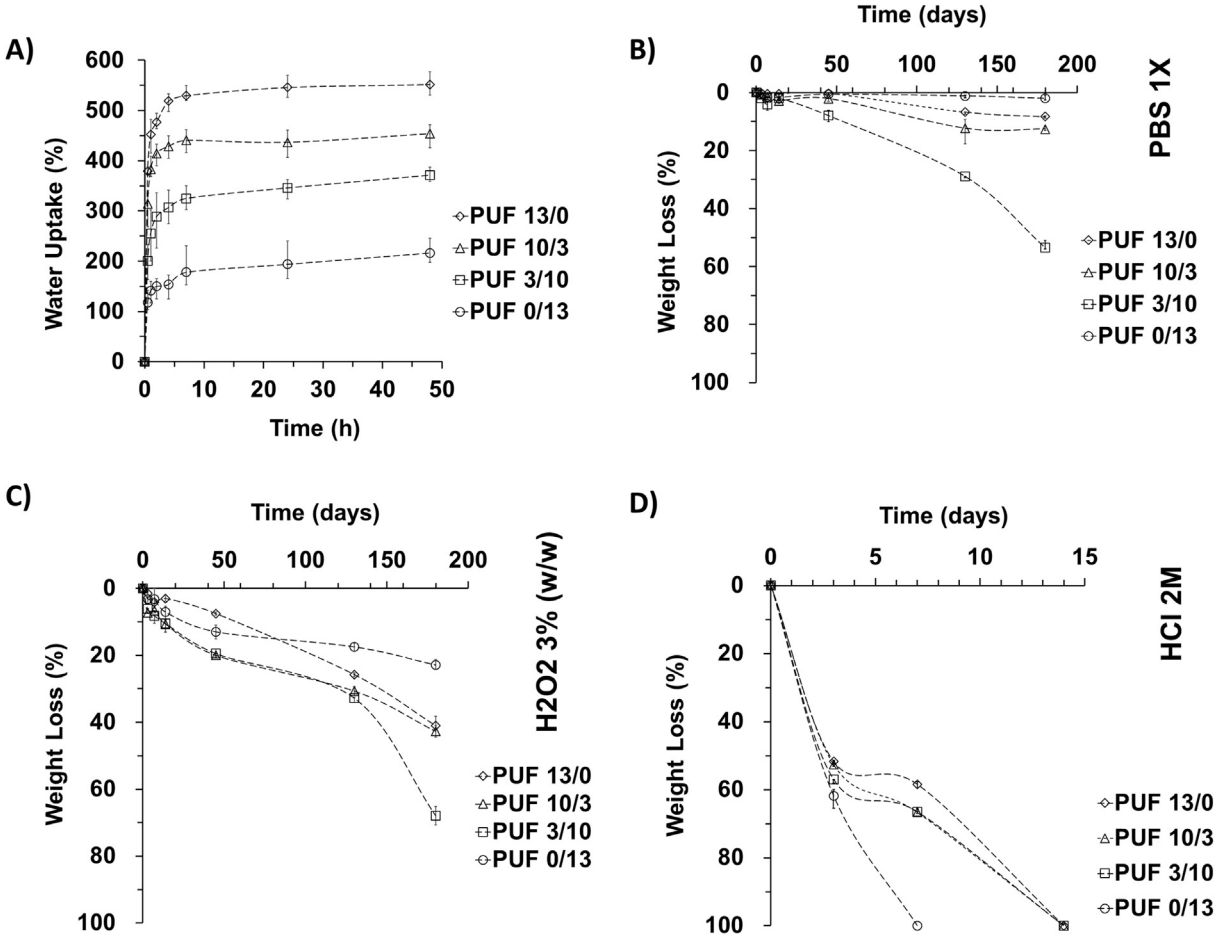

Fig. 2. A) Graphical representation of PUF matrices water uptake capacity overtime, under physiologic conditions (PBS 1X at 37 °C) A), *in vitro* degradation kinetics under physiologic B) and accelerated condition C) and D) (i.e. HCl 2 M and H2O2 3% w/w at 37 °C, respectively).

2.5 Statistical analysis

Results were presented as average values ± standard deviations. Data analysis was performed by one or two-way ANOVA test with Tukey's post-test (GraphPad Prism v5. Software Inc., San Diego, CA, USA) to evaluate statistically significant differences among sample types. The significance threshold was set at 5% (* = $p < 0.05$) and 1% (** = $p < 0.01$). Data are presented as mean values ± standard deviation.

3. Results

3.1. Tuning Physico-chemical and morphological properties of PUF soft scaffolds by varying the PE/PEG-Balance

The employment of cross-linked polyurethanes in the fabrication of biodegradable scaffolds has been so far confined to the field of bone and cartilage tissue engineering, due to their load bearing and creep-resistance properties that are suitable for hard tissue [16,17]. In our previous study, we highlighted the potential of flexible cross-linked polyurethane-based scaffolds for skeletal muscle regeneration, due to their softness ($Ec \leq 10$ kPa) and elasticity (compression strain at failure $\geq 96\%$) [18]. In this work, the mechanical properties of soft PUF were tuned to match that of soft tissue by: (i) employing medium-to-high molecular weight PEG6K and/or PE-diol-13 K segments as chain extenders (6000 < Mn < 13000 Da) and (ii) unbalancing the stoichiometric ratio (between NCO and OH groups), to reduce the stiffness through partial cross-linking of the polymeric chains (Table 1) [19]. Moreover, inspired by Gorna et. al. (2003), we were able to modulate specific physico-chemical properties of the scaffolds (such as the water-uptake capacity and degradation kinetics), by controlling the amount of PEG and/or PE segments in the polymeric structure (Figs. 1 and 2) [20]. HA filler was embedded in the polymeric matrixes of all the 4 soft PUF formulations to (i) enhance the capability to stimulate collagen production [21–23] and (ii) to achieve a secondary micro-porous structure (diameter <5 μm) with the aim to increase the specific surface area and to promote cell infiltration to the matrices [24].

3.1.1. Internal pore morphology

Analyzing the internal morphology of soft PUFs by SEM imaging (Fig. 3), we observed that the formulations containing higher amount of PEG segments (PUF 13/0 and PUF 10/3) exhibited regular and rounded pores resulting from the stabilizing effect of PEG, which acts as a surfactant due to its amphoteric character [25]. Irregular pores and granular surfaces characterized the internal morphology of formulations containing higher amounts of PE seg-

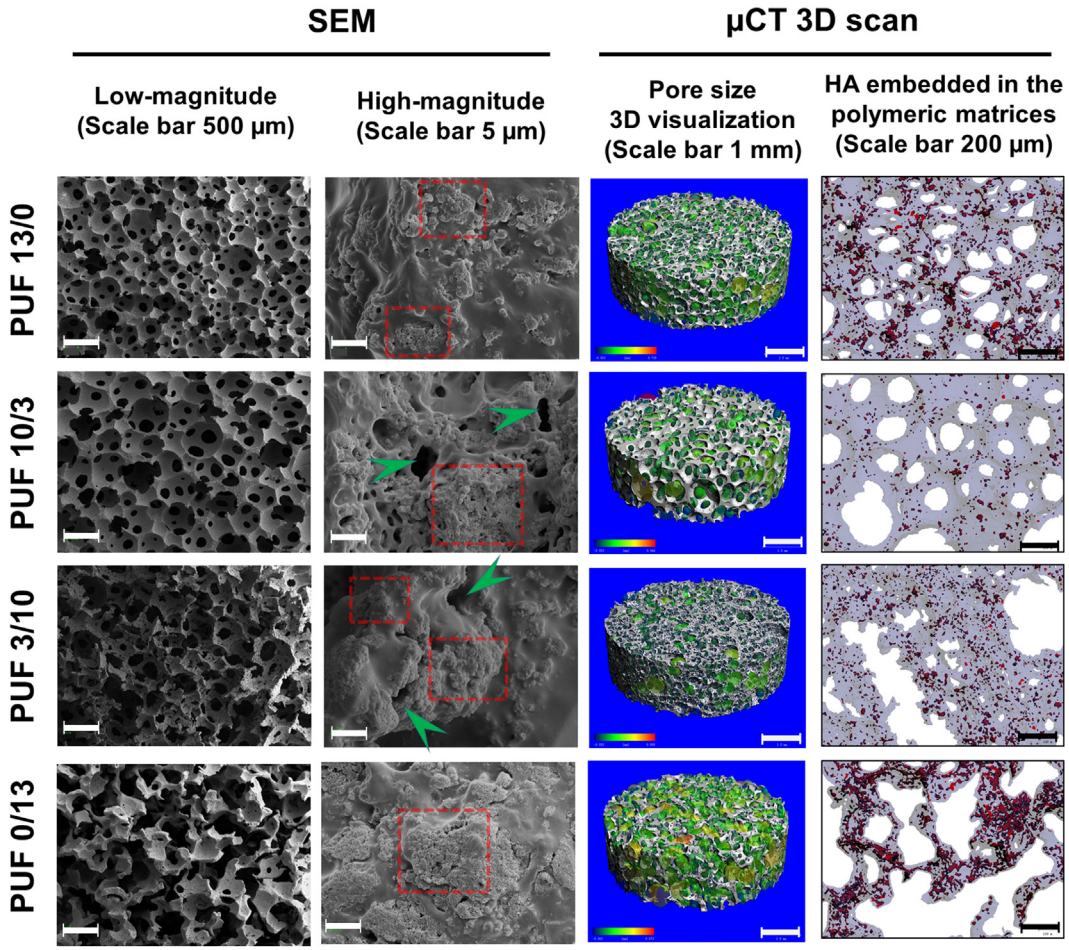

Fig. 3. Morphological characterization of PUF matrices by SEM and μCT 3D scan. From left to right: low magnitude SEM micrographs (scale bar 500 μm); high magnitude SEM micrographs (scale bar 5 μm), where HA cluster where evidenced in dashed red rectangles and micro-pores (dimeter <5 μm) are indicated by light green arrowheads; pore size 3D visualization by μCT 3D scan, where pore size was evidenced by a color scale (from red 0,95 mm to deep blue 0 mm, scale bar 1 mm; visualization of the inorganic filler (HA) distribution in PUF matrices by μCT 3D scan (high magnitude image, scale bar 200 μm). (For interpretation of the references to color in this figure legend, the reader is referred to the web version of this article.)

ments (i.e. PUF 3/10 and PUF 0/13). These results align with those reported by Lee et al (2006), and may be attributed to possible aggregation of PE-containing blocks during the early cross-linking stage of the reaction due to the lower amount of surface active PEG segments [26]. All four formulations were characterized by open interconnected pores, and the average pore size ranged from 200 to 400 μm (Table 2). Morphological characterization by μCT 3D scan shows that all PUF formulations are characterized by similar porosity (85–88%) and local thickness of the walls range of 0.02 and 0.07 mm. Interestingly, the specific surface area of PUF 3/15 was remarkably higher than the other formulations. This can be ascribed to the granular surface and to presence of secondary micro-pores characterizing this formulation (Fig. 3).

HA clusters/aggregates were observed in all soft PUF formulations by SEM (at high magnification) and μCT 3D scan, thereby demonstrating the stability of the inorganic filler in the polymeric matrix after subjection to the purification process.

The beneficial effect of embedded HA filler on the modulation of pore architecture was demonstrated by comparing the specific surface area of PUF 3/10 to the HA-free control formulation: PUF 3/10-zero HA. Results, summarized in Table 2, show that the specific surface area of the HA-free formulation is remarkably lower than all PUF formulations and is 32% of that of PUF 3/10.

3.1.2. Water-uptake capacity

PEG segments enhanced the hydrophilic character of the scaffolds (Fig. 1A) in agreement with previous findings, such as those of in Gould (1989) and Gorna (2003) [20,27]. Water-uptake of the scaffolds followed the trend: PUF 13/0 > PUF 10/3 > PUF 3/10 > PUF 0/13 (Fig. 2A). Nevertheless, water-uptake of the formulation PUF 0/13 was higher than expected (217 ± 25%), considering that it was synthesized using mainly-hydrophobic monomers and precursors. This can be ascribed to the presence of HA fillers embedded in the polymeric matrix, which facilitates diffusion of water into the polymeric matrix, as previously demonstrated by Tihan et. al. (2009) [28]. The water diffusion monitoring test shows that the liquid propagates from the periphery to the center of the scaffold in a time-dependent manner (supplemental data – Fig. S1). Also, water diffusion increased with increasing PEG content. The enhanced hydrophilic character of PEG-containing soft PUF formulations can positively impact body fluids diffusion inside the scaffolds and hence increasing the efficacy of nutrients and oxygen supply to the colonizing cells, especially during the very early stage of tissue regeneration, where the blood vessel network has not yet formed [29].

3.1.3. In vitro degradation kinetics

The test was carried out under physiological (PBS 1X) and accelerated conditions (3% w/w H_2O_2 (ISO10993-13; 1998) and 2 M HCl) in order to more accurately estimate the degradation kinetics in the absence or presence of oxidative stress or inflammation [16]. Interestingly, PUF 0/13 (containing 33% (w/w) degradable PE segments) did not degrade in PBS 1X up to six months (Fig. 2B). This is due to the reduced water penetration through polycaprolactone crystalline domains that slow down the degradation process [30]. Scaffolds containing both PEG and PE segments showed faster

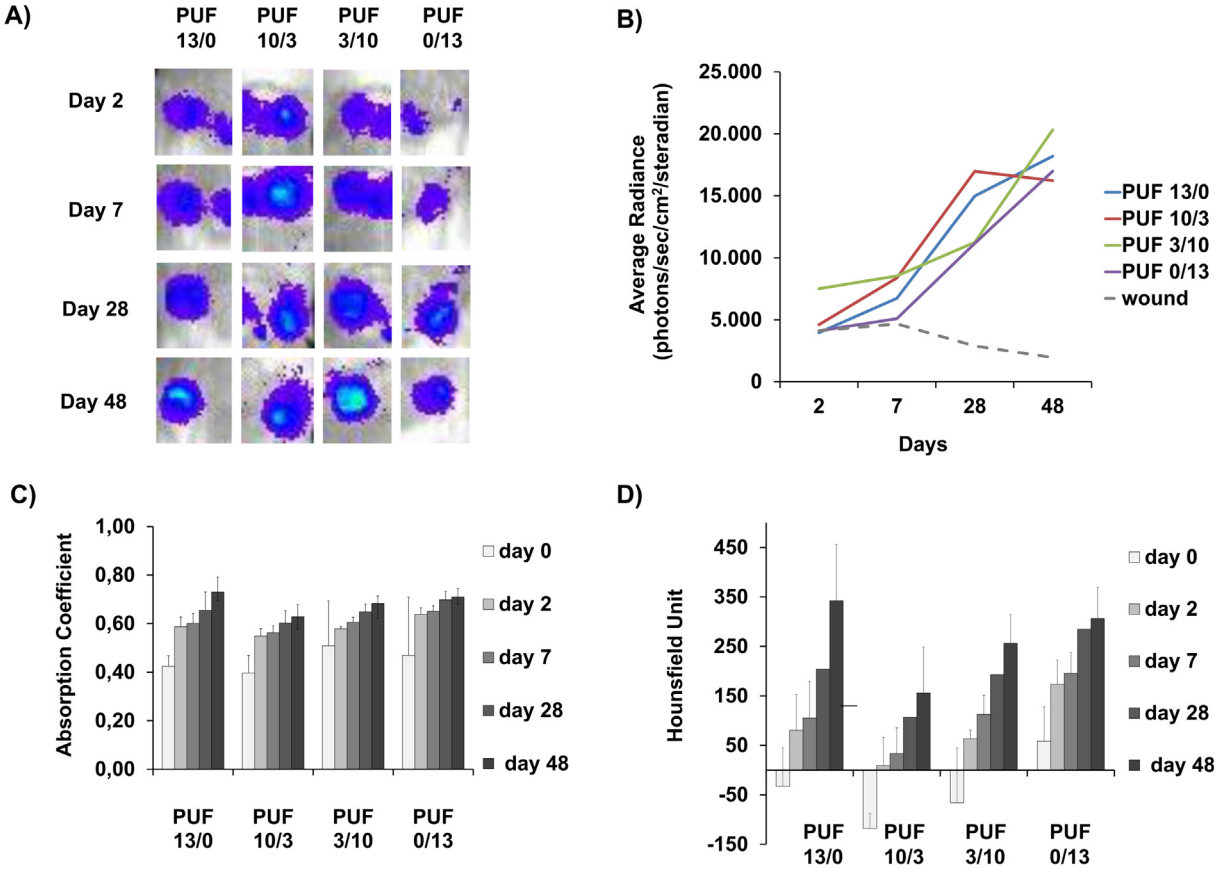

Fig. 4. *In vivo* imaging of inflammation. A) XenoLight Rediject Inflammation Probe luminescent signal for different scaffold formulations and time of acquisitions. B) Bioluminescence quantification of the scaffold imaged in A). μCT scan acquisition. Absorption coefficient C) and Hounsfield units D) of soft PUF scaffolds implanted *in vivo* at 0, 2, 7, 28 and 48 days. No significant differences between the 4 scaffold formulations at the same time point could be observed by μCT scan acquisitions. However, significant differences between time points for the same scaffold formulation were observed D). Values are shown as arithmetic mean ± SD. HU were significantly different for: (i) PUF 13/0 ($p < 0.05$) and PUF 10/3 ($p < 0.01$) (day 2) and (ii) PUF 13/0 ($p < 0.01$), PUF 10/3 ($p < 0.01$) and PUF3/10 ($p < 0.01$) (day 7).

degradation kinetics, which was more evident in PUF 3/10, where more than 50% of the original weight was lost after 6 months. A possible explanation to this result can be ascribed to the chemistry and the pore architecture of PUF 3/10: (i) the presence of hydrophilic PEG segments combined to higher amount of biodegradable PE, characterizing this formulation (i.e. the enhanced hydrophilic character (due to PEG copolymerization) allowed effective hydration of the polymeric matrix and hence boosted the hydrolytic cleavage of polyester segments) [31] and (ii) the remarkably high specific surface area, combined to the lower local thickness of the walls (Table 2) [32]. Soft PUF scaffolds degraded in 3% w/w H_2O_2 according to this trend: PUF 10/3 > PUF 3/10 > PUF 13/0 > PUF 0/13, which is the same as the trend observed for PBS 1X. However, the rate of degradation was faster in oxidative media (Fig. 2C) [33]. In 2 M HCl, complete dissolution of the foams was observed within 7 to 14 days. After 2 h of incubation in HCl 2 M, all PUF scaffolds became transparent due to dissolution of HA filler from the polymeric matrices (Fig. 2D). This result suggests that inflammatory response-related acidosis could accelerate the degradation kinetics [34]. Compression Properties

Static compression tests showed that elastic modulus Ec ranged 7–15 kPa and followed the trend: PUF 13/0 < PUF 10/3 < PUF 3/10 < PUF 0/13. The same trend was observed for compressive stress at 90% strain and from dynamic compression tests (Fig. 1). Considering that all the formulations were synthesized according to similar NCO index (from 77 to 79) and using the same amount of water, stiffness can be attributed solely to poly(ε-caprolactone) hard blocks of PE segments. Regardless, the 4 formulations showed good resilience (i.e. the capability to regain the original shape after deformation) due to the presence of hard and soft segments [35]. More specifically, urea and urethane cross-linking points challenge viscous flow of amorphous soft segments and enable the polymeric chains to regain the original coiled structure [36]. Accordingly, we conclude that soft PUFs can offer adequate mechanical support for soft tissue regeneration *in vivo* [37–39].

3.2. Biological performance in vivo

For the duration of the study, no abnormal clinical signs were observed in implanted mice that appeared in good health, and no local gross adverse reactions were observed (redness, swelling, ulceration) in the skin overlying the scaffolds.

3.2.1. In vivo inflammation and CT evaluation

In this study, chemi-luminescent imaging was performed at 2, 7, 28 and 48 days to dynamically evaluate inflammation in the implanted scaffold. Images in Fig. 4A and B show an increase of inflammation-derived signaling over time following scaffold implantation. Chemiluminescence continued to increase over the duration of the study for PUF 13/0, 3/10 and 0/13. In contrast, PUF 10/3 showed a decreasing trend in inflammation between 28 and 48 days post-implantation.

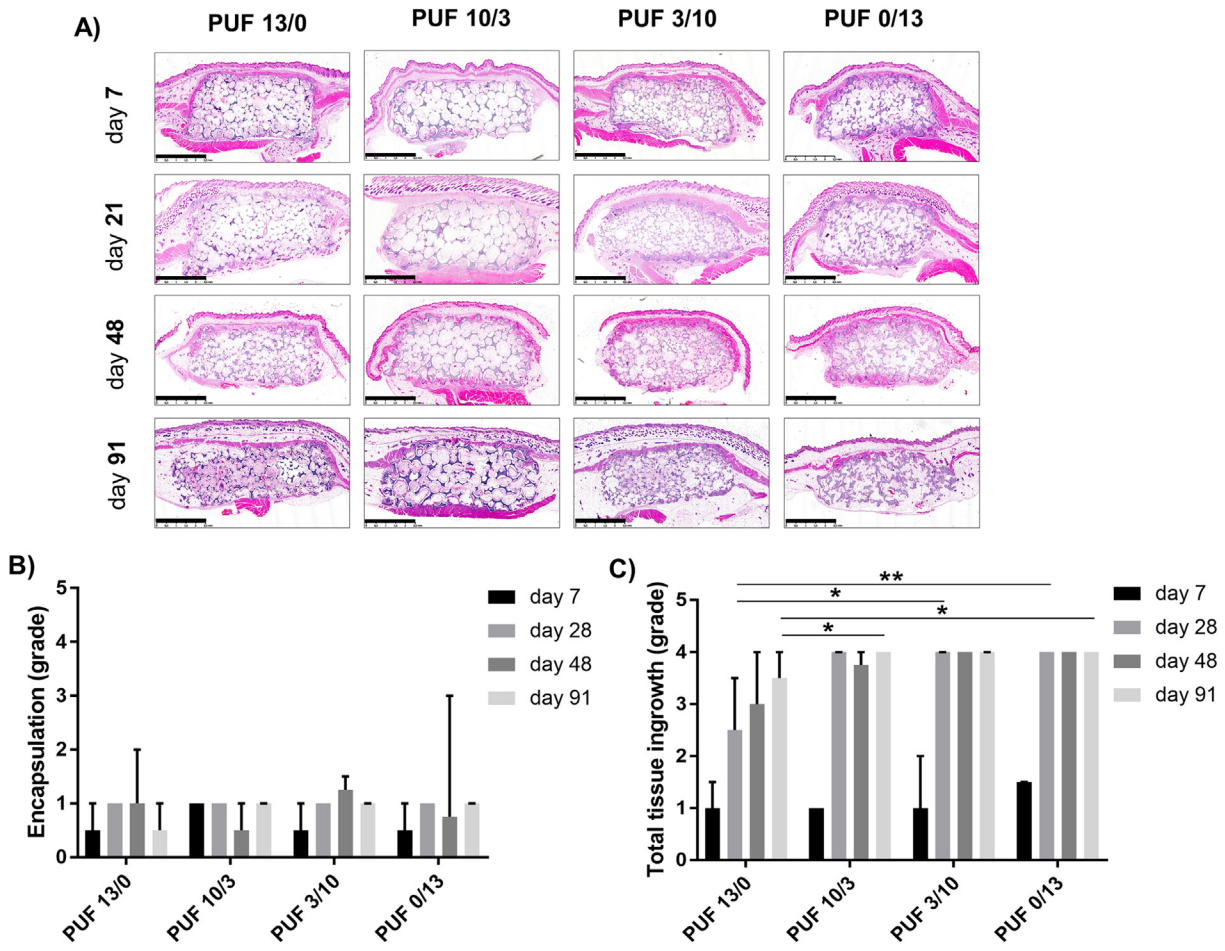

Fig. 5. Histological evaluation of soft PUF scaffolds (13/0; 10/3; 3/10; 0/13) at day 7, 28, 48, 91 after implantation in the subcutis of mice (H&E stain, scale bar = 2.5 mm). A) Representative images show that the porous structure of the scaffolds was maintained up to 91 days. Fibrous encapsulation of the scaffolds was overall partial and mild. Graphical representation of histological scoring for fibrous encapsulation B) and for tissue ingrowth C), at 7, 28, 48, and 91 days.

X-ray absorption and Hounsfield unit (HU) measurements were also performed *in vivo* to better understand tissue density inside and around the scaffolds. As used in practical clinical applications, HU values can be correlated to tissue type and to cell/tissue density [40]. They typically start from negative values at day 0 (due to partial filling of the scaffold with air and water/PBS) and increase gradually over time (due to tissue infiltration and subsequent remodeling) until reaching the range of 100–300 HU, which is characteristic of soft tissue [41]. For all soft PUF formulations, X-ray absorption values and HU increased overtime, suggesting a correlation with increased cellularity due to inflammation processes and tissue formation (Fig. 4C and D) [42].

At the early time points, HU were significantly different for scaffolds having higher amounts of PEG at day 2 (i.e. PUF 13/0 ($p < 0.05$) and PUF 10/3 ($p < 0.01$)) and for the 3 PEG-containing PUF formulations at day 7 (i.e. PUF 13/0 ($p < 0.01$), PUF 10/3 ($p < 0.01$) and PUF3/10 ($p < 0.01$)). This can be attributed to the enhanced hydrophilic character of PEG-containing PUFs which promoted rapid filling with body fluids. At the later time points (day 28 and 48) all scaffolds were significantly different from day 0, indicating increased cellularity over time due to tissue ingrowth.

3.2.2. Histological examination of implanted scaffolds

At all examined time points (7, 28, 48, and 91 days after implantation), soft PUFs were well integrated in the murine subcutaneous tissue (Fig. 5). Mild encapsulation was observed for up to 3 months of implantation, with only a partial fibrous capsule surrounding the scaffolds (Fig. 5A, B). No relevant differences were noted between scaffold types. No necrosis was observed.

Soft PUF scaffolds appeared grey-blue in H&E stained sections. Histological examination confirmed the impact of PE/PEG balance on the modulation of the scaffolds' internal morphology: PUF 13/0 matrix was compact and characterized by regular rounded pore structure, PUF 10/3 matrix was compact-to-granular, and PUF 3/10 and PUF 0/13 matrices were granular with a secondary micro-porous structure (Fig. 6B). These findings are consistent with the differences in internal morphology observed by SEM imaging and μCT 3D scan.

As expected, all soft PUF scaffolds elicited a foreign body response that was mainly characterized by infiltration of macrophages and multinucleated giant cells (MGCs), admixed with granulocytes and lesser numbers of lymphocytes and plasma cells (detailed results of the histological grading of inflammatory cell infiltrates are reported in Supplementary data – Table S2). Evaluation of the inflammatory infiltrate revealed that the total inflammation and MGC scores increased over time for all scaffold types. This is consistent with the results obtained with the Inflammation Probe. Notably there were no relevant differences between scaffold types, except for a higher MGC score in PUF 3/10 vs PUF 13/0 at day 7 and a higher total inflammation in PUF 3/10 vs PUF 13/0 at day 28 (Fig. 6C and D). Large MGCs (with more than 5–10 nuclei) were found already at day 7 only in PUF 3/10 (Fig. 6A), while in the other scaffold types MGCs were found after day 28. Taken together these results indicate that PUF 3/10 induced an early foreign body response compared to the other scaffolds due to its faster degradation kinetics (Fig. 2B, C, D). Literature data indicates that degradation products (such as lactic and glycolic acid) of polyester-based scaffolds may promote an early foreign body response due to possible decreases in pH near the surrounding host tissue [43] The

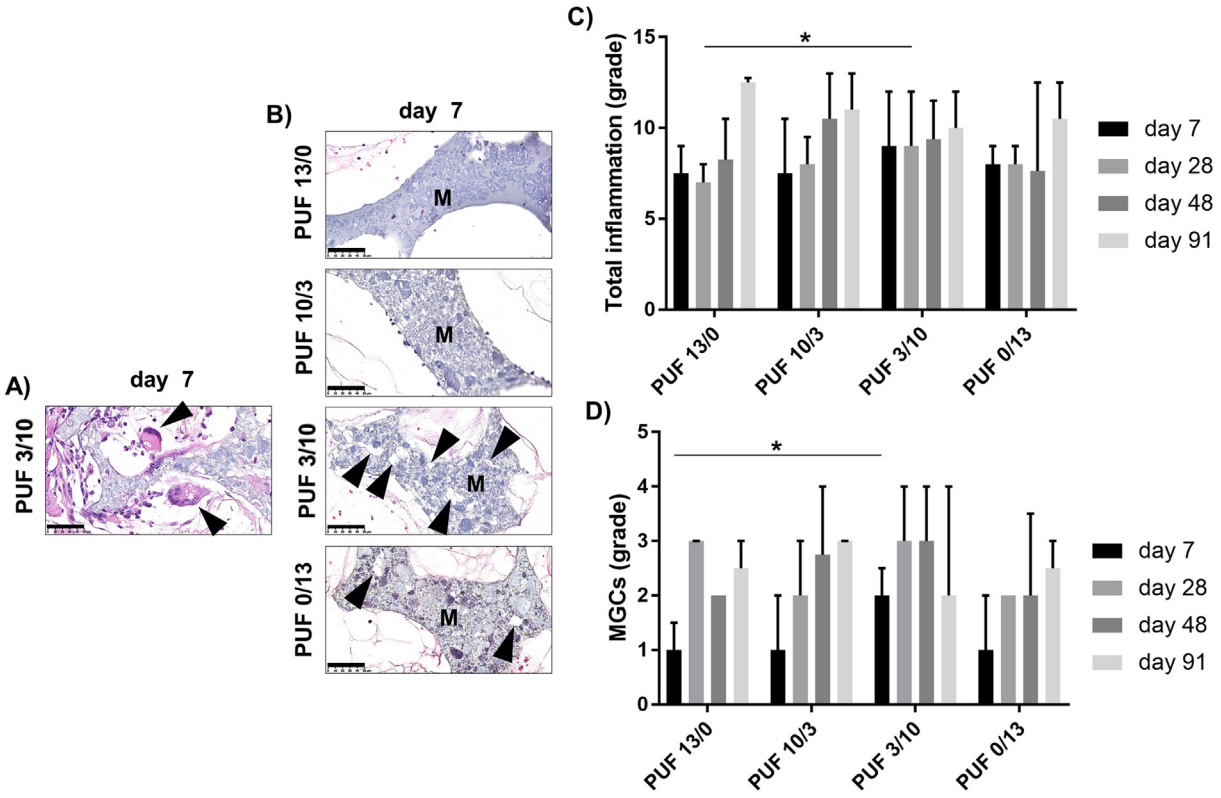

Fig. 6. A) H&E stain of PUF 3/10 explants at day 7 after implantation: only in PUF 3/10 large multinucleated foreign body giant cells (arrowheads) were observed (bar 50 μm). B) Histological appearance of the structure of different PUF scaffolds (13/0; 10/3; 3/10; 0/13) at day 7 after implantation in the subcutis of mice (H&E stain, scale bar = 50 μm). Representative images taken at the center of the scaffolds are shown. PUF 13/0 was characterized by a compact and homogenous matrix (M), while PUF 10/3, PUF 3/10, and PUF 0/13 had a granular matrix. Microporosity (arrowheads) was observed in PUF 3/10 matrix and in PUF 0/13, in minor extent Graphical representation of the histological scoring for total inflammation C) and Multinucleated giant cells MGCs D), at 7, 28, 48, 91 days.

granular surface (Fig. 6B) as well as the low content of anti-fouling PEG segments in PUF 3/10 can also facilitate protein adsorption and monocyte adhesion to scaffold during the very first days after implantation [44]. The extent of foreign body response of this formulation is considered modest, as no signs of acute or chronic inflammation were observed in mice during implantation (such as febrile episodes, redress, swelling, etc.) (Figs. 7 and 8A). Future studies investigating quantification of cytokine expression in the tissue surrounding the implanted scaffold would be useful to more extensively assess the biocompatibility of this biomaterial [45].

Regarding tissue ingrowth into the scaffolds, at day 7 pores were only partially infiltrated starting from the periphery, while at day 28 after implantation tissue infiltration of scaffolds was almost complete, except for PUF 13/0 where colonization was a slower and more gradual process (Fig. 5C). Notably, the growing tissue within the pores was impacted by the chemistry of soft PUFs. Cell adhesion to the matrix was observed only in those scaffolds having low-to-zero PEG content (PUF 3/10 and 0/13), while in PUF scaffolds having high PEG content (PUF 13/0 and 10/3) the tissues did not adhere to the surface of the matrix (Fig. 7A). The lack of cell adhesion observed in soft PUF scaffolds with high PEG content was likely related to its antifouling properties and could be responsible also for the delayed tissue colonization of PUF 13/0 [46,47].

In addition to cell adhesion to the polymeric matrices, in scaffold PUF 3/10 there was also early cellular infiltration of the matrix starting at day 7, which resulted in its later partial fragmentation (Fig. 7A – 91 days). Cellular infiltration of PUF 3/10 scaffolds (Fig. 6B) was likely encouraged by the higher susceptibility to undergo hydrolytic cleavage of ester groups by hydrolysis in aqueous media - observed in *in vitro* tests- (Fig. 2B) and by the relatively low local thickness of the polymeric matrix, as well as the higher surface area, distinguishing this formulation (Table 2). After 3 months of implantation, the matrices PUF 13/0 and PUF 10/3 maintained the initial thickness of the pore walls, indicating slow degradation *in vivo*. This aligns with degradation kinetics *in vitro* results, where the matrices lost <10% of the original weight in 3 months (Fig. 2B).

In all scaffold types, the most prevalent tissue detected within the pores was a loose fibromyxoid tissue composed of spindle-to-stellate cells occasionally embedded in a floccular extracellular matrix (consistent with a poorly differentiated mesenchymal tissue) that was present at all time points of examination and increased from day 7 to day 48. Interestingly, at day 91 the fibromyxoid tissue was partially replaced by a differentiated adipose tissue that extended from the periphery to the inner core of the scaffolds (Figs. 7 and 8A).

The extensive tissue ingrowth observed in all soft PUFs was supported by well-developed and functional blood vessels filled with erythrocytes, extending deep into the inner core of the scaffolds (Fig. 8A2 and A6). Occasionally, a few preadipocytes were also detected in the most central regions of the scaffolds (Fig. 8A5).

Quantification of total fibrillar collagen of the colonizing tissue within the scaffolds at day 91 by picrosirius red staining showed that collagen deposition in PUF 3/10 matrix was slightly lower than the other formulations; however, the difference was not statistically significant (Fig. 8B and D). Considering that: (i) the non-cell component of soft tissue, is basically composed of collagenous

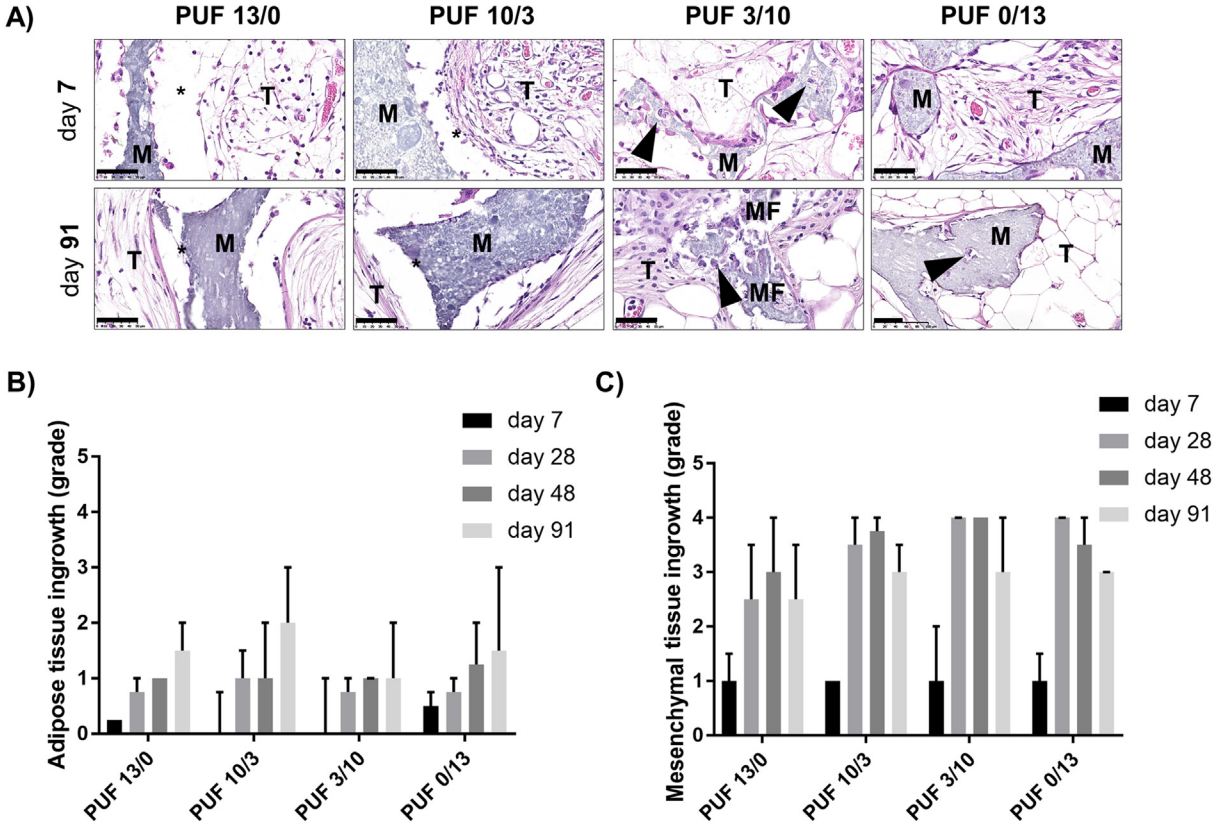

Fig. 7. A) Cell behavior (adhesion to the matrix surface and infiltration into the matrix) after tissue colonization of the 4 soft PUFs at day 7 and 91 after implantation in the subcutis of mice (H&E stain, scale bar = 50 μm). In PUF 13/0 and PUF 10/3, cells did not adhere to the matrix surface leaving an empty space (*) between the newformed tissue (T) grown within pores and the scaffold matrix (M). In PUF 3/10 and PUF 0/13, cell adhesion was present and cell infiltration occurred in scaffold 3/10 starting from day 7 and resulting in partial fragmentation of the scaffold matrix (MF) at day 91. Cell infiltration to the matrix (arrowheads) was also occasionally observed in the other soft PUFs (but less in PUF 0/13), starting from day 48 after implantation. Graphical representation of the histological scoring for mesenchymal tissue ingrowth B), adipose tissue ingrowth C), at 7, 28, 48, 91 days.

extracellular matrix, which structure evolves from fibrillar to laminar during the process of adipogenic differentiation, (ii) the amount of fibrillar collagen in the extracellular matrices is about 7–10% and (iii) the abundant presence of mature adipocytes, we can conclude that the composition of the newly regenerated tissue through PUF matrices complies to the characteristics of the target soft tissue [48].

4. Discussion

In this study, we developed a series of biodegradable poly (urethane)-based scaffolds, featured by an exceptional combination between softness and high resilience, for soft tissue. PUF matrices were designed to overcome specific limitation of the so far developed alternatives, in particular: the uncontrolled degradation kinetics *in vivo* and the lack of adequate mechanical support during the process of soft tissue regeneration of clinically relevant volumes. Softness and high resilience were achieved according to a well-defined synthetic approach, which is mainly based on the copolymerization with soft amorphous polymeric segments and the adoption of an unbalanced stoichiometry between NCO and OH groups. Accordingly, we could extend the employment of this class of biomaterials -which was so far confined for bone and osteochondral tissue regeneration- to other types of connective tissue. Exploring the potential of soft PUFs as scaffold for soft tissue regeneration proceeded in two directions: (i) identifying the impact of specific physico-chemical properties on the biological performance *in vivo* and by (ii) understanding the mechanism according which soft tissue regeneration occurs throughout the scaffold over time. To this aim, specific physico-chemical properties (e.g. hydrophilic character, degradation kinetics, softness and surface roughness) of 4 soft PUF formulations were finely tuned by varying the ratio between PEG and PE segments. Previous investigations showed that collagen contributes considerably to the non-cell mass of adipose tissue [48], where adipocytes are surrounded by extracellular matrix ECM where collagen IV is a major component [49]. The regulatory role of collagen-based ECM during adipogenic differentiation has been also assessed [50,51]. The stimulation of collagen production enables recapitulation of suitable microenvironment for adipose tissue survival and hence boost the entire process of soft tissue regeneration [52]. The capability of hydroxyapatite to stimulate the production of collagen IV, was reported by: Berlin et al. (2008) [53] and recently by Simunovic et. al. (2017) [54] and was object of many patents [55,56] and commercially available products [22,23]. Accordingly, HA was embedded in the polymeric matrices of the 4 PUF formulations. The

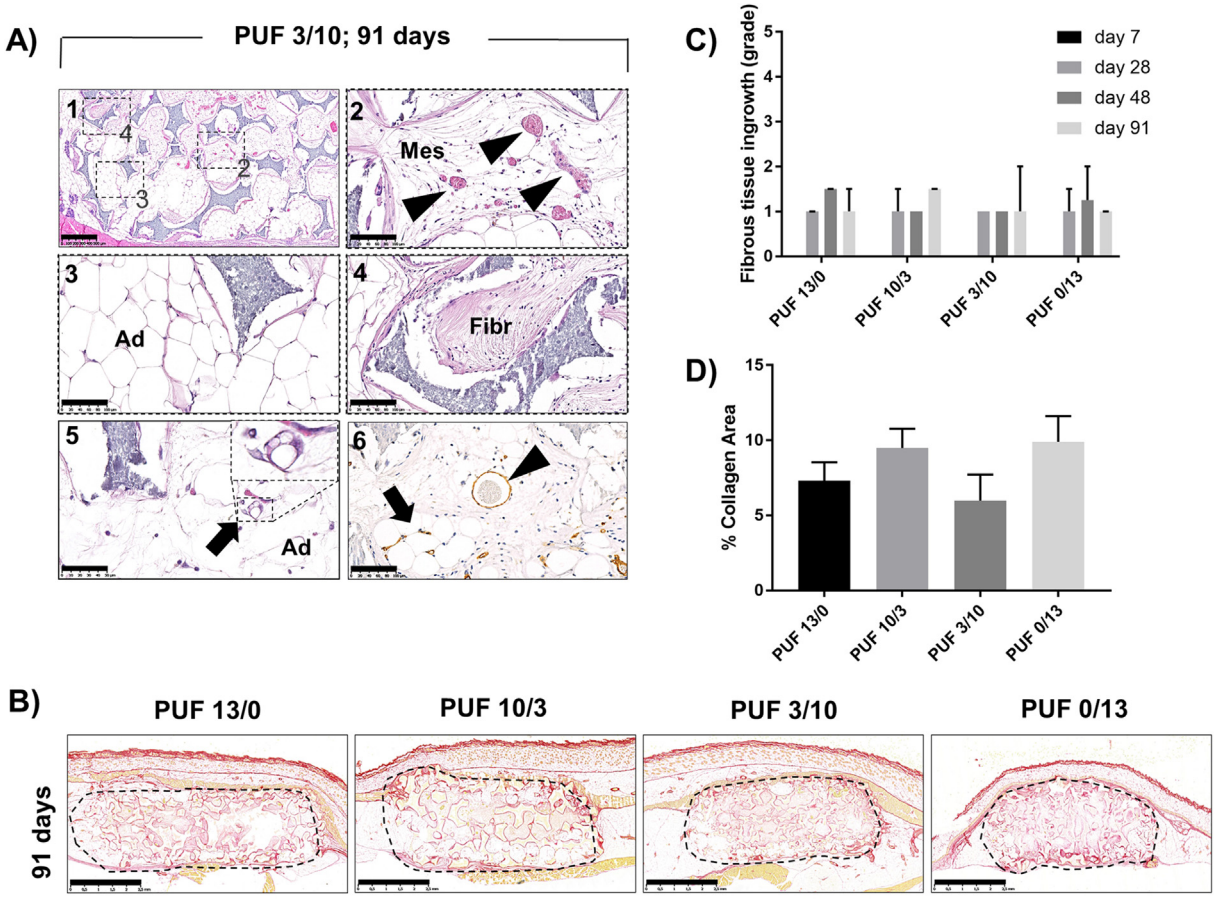

Fig. 8. A) PUF3/10 at day 91 post implantation: A1) the scaffold was well colonized by neoformed tissue grown within pores (H&E stain, scale bar = 500 μm). A2) Undifferentiated mesenchymal tissue (Mes) with numerous blood vessels (arrowheads) (H&E stain, scale bar = 100 μm). A3) Mature adipose tissue (H&E stain, scale bar = 100 μm). A4) Fibrous tissue (Fibr) (H&E stain, scale bar = 100 μm). A5) rare preadipocytes were found at day 91 in the most central areas of the scaffolds (arrow) (H&E stain, scale bar = 50 μm). A6) CD31-positive endothelial cells lining a blood vessel filled with eythrocytes (immunoperoxidase staining, scale bar = 50 μm). B) Picrosirius red staining for the evaluation of collagen deposition within the scaffold area (dotted line) at day 91 post implantation in the subcutis of mice. Representative images are shown. (scale bar = 2.5 mm). C) Graphical representation of the histological scoring for fibrous tissue ingrowth, at 7, 28, 48, 91 days. D) % area of collagen deposition within the scaffolds after 91 days of implantation quantified by using the ImageJ analysis program v1.49 (http://rsb.info.nih.gov/ij/) selecting as Region of Interest (ROI) the area occupied by the implanted scaffold (dotted line in (B)). (For interpretation of the references to color in this figure legend, the reader is referred to the web version of this article.)

impact on biological performance *in vivo* was investigated via implantation in a murine model. The biological performance of soft PUF formulations was impacted by the intrinsic physico-chemical properties, especially at early time points after implantation. More specifically, HU measurements confirmed that the hydrophilic character of PEG-containing PUFs allowed rapid filling with body fluids during the first few days after implantation. Histological analyses confirmed that tissue ingrowth proceed slower in PUF 13/0 scaffolds (having only PEG chain extender segments and no PE). Moreover, lack of cell adhesion was observed in scaffolds having higher amounts of PEG segments (i.e. PUF 13/0 and PUF 10/3). Accordingly, we suggest keeping the amount of PEG chain extender segments to the minimum necessary for the enhancement of the scaffolds hydrophilic character to avoid the undesired anti-fouling effect. On the other hand, the fast degradation kinetics scaffolds, the granular micro-porous surface, and the higher specific surface area of PUF 3/10 enabled cell infiltration to the matrix, during the first month of implantation, leading to better integration with the surrounding tissue. Therefore, we conclude that the best PEG/PE balance was that of PUF 3/10 (less PEG and more PE). Investigating the *in vivo* biological performance at different time points, allowed better understanding to the mechanism of soft tissue regeneration within the cell-free scaffold. We observed that undifferentiated mesenchymal cells were able to gradually infiltrate through thanks to the enhanced hydrophilic character and to the highly interconnected porous structure. Cell infiltration proceeded through the periphery towards the center of the scaffold. The formation of well differentiated adipose tissue was found to proceed in a step-wise fashion and requires functional and well-formed vascular network to supported cell viability.

5. Conclusion

The step-wise process of adipose tissue regeneration is unlikely compatible with the fast and uncontrolled degradation of natural origin scaffolds. The development of synthetic alternatives can pave the way to achieve an effective soft tissue repair and reconstruction, especially for clinically relevant volumes.

In this study, we developed a flexible biodegradable polyurethane-based scaffold and explored its potential as cell-free matrix for soft tissue regeneration by establishing causal relationship between the intrinsic physico-chemical properties and the biological performance, *in vivo*. The physico-chemical properties (i.e. hydrophilic character, degradation kinetics, softness and surface roughness) of 4 soft PUF formulations were finely tuned by varying the amount of PEG and PE segments in the polymeric structure. The enhanced hydrophilic character of PEG-containing soft PUFs favored efficacious diffusion of body fluids during the very few days after implant, however a special attention must be paid while balancing the amount of PEG in polymeric structure to minimize associated anti-fouling effect. With a view to achieve natural regeneration of clinically relevant volumes, further investigations are necessary to assess the impact of internal morphology (in terms of pore size, interconnection between pores, matrices local thickness, porosity and specific surface area) on the viability of colonizing tissue. In this context, authors do not exclude that fluidic channel network combined to a well-interconnected porous structure would increase the chance of tissue survival in the central part of scaffold. Additional *in vivo* tests in other rodent and non-rodent models are in progress to support findings of this study and to evaluate the scaffolds biological performance in more challenging scenarios, in terms of animals' sensitivity and the volume of regenerated soft tissue.

6. Author contribution

The manuscript was written through contributions of all authors. All authors have given approval to the final version of the manuscript. IG designed the study, produced soft PUF scaffolds and wrote the manuscript. MT performed the biological validation study and coordinated the *in vivo* tests. MCT collaborated to the biological validation tests. FM performed physico-chemical characterizations. CR performed histological analyses. CM and LO performed *in vivo* imaging with inflammation probe and μCT scan. SG collaborated to data analyses and interpretation and revised the manuscript. AT and CL revised the manuscript and coordinated the study.

7. Funding

This work was partially funded by Regione Lombardia with POR FESR 2007–2013 resources (grant ID: ATP 2009, No. 13396272).

8. Disclosures

The authors of this manuscript have the following potential competing interests: IG, MT, AT, FM are inventors of the patent entitled Foamed polyurethane polymers for the regeneration of connective tissue # WO2015162523 A1 (also published as CA2944841A1, EP3134447A1, US20170044344). This patent has been licensed to Tensive S.r.l. IG, MT, AT, FM are co-founders and share-holders of Tensive S.r.l. The patent and its licensing, do not alter our adherence to Acta Biomaterialia policies on sharing data and materials. The other authors have no competing interests to declare.

Acknowledgements

Authors kindly acknowledge the contribution of Mr Martino Alfredo Cappelluti to the biological validation tests and Dr Stefania Riboldi for the scientific discussion.

Appendix A. Supplementary data

Supplementary data associated with this article can be found, in the online version, at https://doi.org/10.1016/j.actbio.2018.04.011.

References

[1] R.J. Ross, R. Shayan, K.L. Mutimer, M.W. Ashton, Autologous fat grafting: current state of the art and critical review, Ann. Plast. Surg. 73 (2014) 352–357, https://doi.org/10.1097/SAP.0b013e31827aeb51.
[2] E. Korurer, H. Kenar, E. Doger, E. Karaoz, Production of a composite hyaluronic acid/gelatin blood plasma gel for hydrogel-based adipose tissue engineering applications, J. Biomed. Mater. Res. Part A. 102 (2014) 2220–2229, https://doi.org/10.1002/jbm.a.34901.
[3] E. Kon, G. Filardo, A. Roffi, L. Andriolo, M. Marcacci, New trends for knee cartilage regeneration: from cell-free scaffolds to mesenchymal stem cells, Curr. Rev. Musculoskelet. Med. 5 (2012) 236–243, https://doi.org/10.1007/s12178-012-9135-x.
[4] J. Ankrum, J.M. Karp, Mesenchymal stem cell therapy: two steps forward, one step back, Trends Mol. Med. 16 (2010) 203–209, https://doi.org/10.1016/j.molmed.2010.02.005.
[5] E. Rossi, I. Gerges, A. Tocchio, M. Tamplenizza, P. Aprile, C. Recordati, F. Martello, I. Martin, P. Milani, C. Lenardi, Biologically and mechanically driven design of an RGD-mimetic macroporous foam for adipose tissue engineering applications, Biomaterials. 104 (2016), https://doi.org/10.1016/j.biomaterials.2016.07.004.
[6] R.M. Shanti, S. Janjanin, W.-J. Li, L.J. Nesti, M.B. Mueller, M.B. Tzeng, R.S. Tuan, In vitro adipose tissue engineering using an electrospun nanofibrous scaffold, Ann. Plast. Surg. 61 (2008) 566–571, https://doi.org/10.1097/SAP.0b013e31816d9579.
[7] D.P. Martin, S.F. Williams, Medical applications of poly-4-hydroxybutyrate: a strong flexible absorbable biomaterial, Biochem. Eng. J. 16 (2003) 97–105, https://doi.org/10.1016/S1369-703X(03)00040-8.
[8] C.G. Jeong, S.J. Hollister, Mechanical, permeability, and degradation properties of 3D designed poly(1,8 octanediol-co-citrate) scaffolds for soft tissue engineering, J. Biomed. Mater. Res. Part B Appl. Biomater. 9999B (2010), https://doi.org/10.1002/jbm.b.31568.
[9] S.-W. Kang, S.-W. Seo, C.Y. Choi, B.-S. Kim, Porous poly(lactic-co-glycolic acid) microsphere as cell culture substrate and cell transplantation vehicle for

adipose tissue engineering, Tissue Eng. Part C Methods. 14 (2008) 25–34, https://doi.org/10.1089/tec.2007.0290.
[10] Y. Wang, G.A. Ameer, B.J. Sheppard, R. Langer, A tough biodegradable elastomer, Nat. Biotechnol. 20 (2002) 602–606, https://doi.org/10.1038/nbt0602-602.
[11] R. Rai, M. Tallawi, A. Grigore, A.R. Boccaccini, Synthesis, properties and biomedical applications of poly(glycerol sebacate) (PGS): a review, Prog. Polym. Sci. 37 (2012) 1051–1078, https://doi.org/10.1016/J.PROGPOLYMSCI.2012.02.001.
[12] J.M. Kemppainen, S.J. Hollister, Tailoring the mechanical properties of 3D-designed poly(glycerol sebacate) scaffolds for cartilage applications, J. Biomed. Mater. Res. Part A. 94A (2010) 9–18, https://doi.org/10.1002/jbm.a.32653.
[13] P. Gentile, V. Chiono, I. Carmagnola, P. Hatton, An overview of poly(lactic-co-glycolic) acid (PLGA)-based biomaterials for bone tissue engineering, Int. J. Mol. Sci. 15 (2014) 3640–3659, https://doi.org/10.3390/ijms15033640.
[14] B. Saad, Y. Kuboki, M. Welti, G.K. Uhlschmid, P. Neuenschwander, U.W. Suter, DegraPol-foam: a degradable and highly porous polyesterurethane foam as a new substrate for bone formation, Artif. Organs. 24 (2000) 939–945, https://doi.org/10.1046/j.1525-1594.2000.06664.x.
[15] M. Tamplenizza, A. Tocchio, I. Gerges, F. Martello, C. Martelli, L. Ottobrini, G. Lucignani, P. Milani, C. Lenardi, In vivo imaging study of angiogenesis in a channelized porous scaffold, Mol. Imaging. 14 (2015). 7290201500011 10.2310/7290.2015.00011.
[16] I. Gerges, M. Tamplenizza, S. Lopa, C. Recordati, F. Martello, A. Tocchio, L. Ricotti, C. Arrigoni, P. Milani, M. Moretti, C. Lenardi, Creep-resistant dextran-based polyurethane foam as a candidate scaffold for bone tissue engineering: Synthesis, chemico-physical characterization, and in vitro and in vivo biocompatibility, Int. J. Polym. Mater. Polym. Biomater. 65 (2016), https://doi.org/10.1080/00914037.2016.1163565.
[17] S.L. Cooper, J. Guan (Eds.), Advances in polyurethane biomaterials, 1st ed., Woodhead Publishing Series in Biomaterials, https://www.elsevier.com/books/advances-in-polyurethane-biomaterials/cooper/978-0-08-100614-6, 2016.
[18] L. Vannozzi, L. Ricotti, T. Santaniello, T. Terencio, R. Oropesa-Nunez, C. Canale, F. Borghi, A. Menciassi, C. Lenardi, I. Gerges, 3D porous polyurethanes featured by different mechanical properties: characterization and interaction with skeletal muscle cells, J. Mech. Behav. Biomed. Mater. 75 (2017) 147–159, https://doi.org/10.1016/j.jmbbm.2017.07.018.
[19] I. Gerges, M. Tamplenizza, E. Rossi, A. Tocchio, F. Martello, C. Recordati, D. Kumar, N.R. Forsyth, Y. Liu, C. Lenardi, A tailor-made synthetic polymer for cell encapsulation: design rationale, synthesis, chemical-physics and biological characterizations, Macromol. Biosci. 16 (2016) 870–881, https://doi.org/10.1002/mabi.201500386.
[20] K. Gorna, S. Gogolewski, Preparation, degradation, and calcification of biodegradable polyurethane foams for bone graft substitutes, J. Biomed. Mater. Res. A. 67 (2003) 813–827, https://doi.org/10.1002/jbm.a.10148.
[21] K.M. Coleman, R. Voigts, D.P. Devore, P. Termin, W.P. Coleman III, Neocollagenesis after Injection of calcium hydroxylapatite composition in a canine model, Dermatologic Surg. 34 (2008) S53–S55, https://doi.org/10.1111/j.1524-4725.2008.34243.x.
[22] P.F. Jacovella, Use of calcium hydroxylapatite (Radiesse) for facial augmentation, Clin. Interv. Aging. 3 (2008) 161–174.
[23] P.F. Jacovella, C.B. Peiretti, D. Cunille, M. Salzamendi, S.A. Schechtel, Long-lasting results with hydroxylapatite (radiesse) facial filler, Plast. Reconstr. Surg. 118 (2006) 15S–21S, https://doi.org/10.1097/01.prs.0000234902.61284.c9.
[24] M.C. Wake, C.W. Patrick, A.G. Mikos, Pore morphology effects on the fibrovascular tissue growth in porous polymer substrates, Cell Transplant. 3 (1994) 339–343, https://doi.org/10.1177/096368979400300411.
[25] A. Cervantes-Martínez, A. Maldonado, Foaming behaviour of polymer–surfactant solutions, J. Phys. Condens. Matter. 19 (2007) 246101, https://doi.org/10.1088/0953-8984/19/24/246101.
[26] K.B. Yoon, Y.J. Lee, Effect of composition of polyurethane foam template on the morphology of silicalite foam, Microporous Mesoporous Mater. 88 (2006) 176–186, https://doi.org/10.1016/J.MICROMESO.2005.08.039.
[27] S.D.R. Francis E. Gould, Ellen K. Morgan, Hydrophilic polyurethane composition, US4810582 A, 1988.
[28] D.L. Teodora, Gratiela Tihan, Mioara Daniela Ionita, Roxana Gabriela Popescu, Effect of hydrophilic-hydrophobic balance on biocompatibility of poly(methyl methacrylate) (PMMA)-hydroxyapatite (HA) composites, Mater. Chem. Phys. 118 (2009) 265–269, https://doi.org/10.1016/J.MATCHEMPHYS.2009.03.019.
[29] S.H. Oh, J.H. Lee, Hydrophilization of synthetic biodegradable polymer scaffolds for improved cell/tissue compatibility, Biomed. Mater. 8 (2013) 14101.
[30] J.R.S.J. Fernández, A. Larrañaga, A. Etxeberría, Effects of chain microstructures and derived crystallization capability on hydrolytic degradation of poly(l-lactide/ε-caprolactone) copolymers, Polym. Degrad. Stab. 98 (2013) 481–489, https://doi.org/10.1016/J.POLYMDEGRADSTAB.2012.12.014.
[31] S.G. Katarzyna Gorna, In vitro degradation of novel medical biodegradable aliphatic polyurethanes based on ϵ-caprolactone and Pluronics® with various hydrophilicities, Polym. Degrad. Stab. 75 (2002) 113–122, https://doi.org/10.1016/S0141-3910(01)00210-5.
[32] J.-A. Kim, J. Lim, R. Naren, H. Yun, E.K. Park, Effect of the biodegradation rate controlled by pore structures in magnesium phosphate ceramic scaffolds on bone tissue regeneration in vivo, Acta Biomater. 44 (2016) 155–167, https://doi.org/10.1016/j.actbio.2016.08.039.
[33] J.P. Santerre, K. Woodhouse, G. Laroche, R.S. Labow, Understanding the biodegradation of polyurethanes: from classical implants to tissue engineering materials, Biomaterials. 26 (2005) 7457–7470, https://doi.org/10.1016/j.biomaterials.2005.05.079.
[34] A. Lardner, The effects of extracellular pH on immune function, J. Leukoc. Biol. 69 (2001) 522–530.
[35] J.C. Moreland, G.L. Wilkes, R.B. Turner, Viscoelastic behavior of flexible slabstock polyurethane foam as a function of temperature and relative humidity. II. Compressive creep behavior, J. Appl. Polym. Sci. 52 (1994) 569–576, https://doi.org/10.1002/app.1994.070520412.
[36] W. Wang, Y. Jin, P. Ping, X. Chen, X. Jing, Z. Su, Structure evolution in segmented poly(ester urethane) in shape-memory process, Macromolecules. 43 (2010) 2942–2947, https://doi.org/10.1021/ma902781e.
[37] J.F. Ana Paula Pêgo, André A. Poot, Dirk W. Grijpma, Biodegradable elastomeric scaffolds for soft tissue engineering, J. Control. Release. 87 (2003) 69–79, https://doi.org/10.1016/S0168-3659(02)00351-6.
[38] N.A.F. Kerstyn Comley, A micromechanical model for the Young's modulus of adipose tissue, Int. J. Solids Struct. 47 (2010) 2982–2990, https://doi.org/10.1016/J.IJSOLSTR.2010.07.001.
[39] A. Samani, J. Zubovits, D. Plewes, Elastic moduli of normal and pathological human breast tissues: an inversion-technique-based investigation of 169 samples, Phys. Med. Biol. 52 (2007) 1565–1576, https://doi.org/10.1088/0031-9155/52/6/002.
[40] U. Schneider, E. Pedroni, A. Lomax, The calibration of CT Hounsfield units for radiotherapy treatment planning, Phys. Med. Biol. 41 (1996) 111–124.
[41] S. Baba, H.A. Jacene, J.M. Engles, H. Honda, R.L. Wahl, CT Hounsfield units of brown adipose tissue increase with activation: preclinical and clinical studies, J. Nucl. Med. 51 (2010) 246–250, https://doi.org/10.2967/jnumed.109.068775.
[42] B. Bashist, H.L. Hecht, W.D. Harley, Computed tomographic demonstration of rapid changes in fatty infiltration of the liver, Radiology. 142 (1982) 691–692, https://doi.org/10.1148/radiology.142.3.7063686.
[43] W. Ji, F. Yang, H. Seyednejad, Z. Chen, W.E. Hennink, J.M. Anderson, J.J.J.P. van den Beucken, J.A. Jansen, Biocompatibility and degradation characteristics of PLGA-based electrospun nanofibrous scaffolds with nanoapatite incorporation, Biomaterials. 33 (2012) 6604–6614, https://doi.org/10.1016/j.biomaterials.2012.06.018.
[44] J.M. Anderson, A. Rodriguez, D.T. Chang, Foreign body reaction to biomaterials, Semin. Immunol. 20 (2008) 86–100, https://doi.org/10.1016/j.smim.2007.11.004.
[45] R.J. Schutte, L. Xie, B. Klitzman, W.M. Reichert, In vivo cytokine-associated responses to biomaterials, Biomaterials. 30 (2009) 160–168, https://doi.org/10.1016/j.biomaterials.2008.09.026.
[46] Sadhana Sharma, Robert W. Johnson, Tejal A. Desai, XPS and AFM analysis of antifouling PEG interfaces for microfabricated silicon biosensors, Biosens. Bioelectron. 20 (2004) 227–239, https://doi.org/10.1016/J.BIOS.2004.01.034.
[47] Jeffrey L. Dalsin, Phillip B. Messersmith, Bioinspired antifouling polymers, Mater. Today. 8 (2005) 38–46, https://doi.org/10.1016/S1369-7021(05)71079-8.
[48] E.C.M. Mariman, P. Wang, Adipocyte extracellular matrix composition, dynamics and role in obesity, Cell. Mol. Life Sci. 67 (2010) 1277–1292, https://doi.org/10.1007/s00018-010-0263-4.
[49] C. Pierleoni, F. Verdenelli, M. Castellucci, S. Cinti, Fibronectins and basal lamina molecules expression in human subcutaneous white adipose tissue, Eur. J. Histochem. 42 (1998) 183–188.
[50] Y. Aratani, Y. Kitagawa, Enhanced synthesis and secretion of type IV collagen and entactin during adipose conversion of 3T3-L1 cells and production of unorthodox laminin complex, J. Biol. Chem. 263 (1988) 16163–16169.
[51] I. Nakajima, H. Aso, T. Yamaguchi, K. Ozutsumi, Adipose tissue extracellular matrix: newly organized by adipocytes during differentiation, Differentiation. 63 (1998) 193–200, https://doi.org/10.1111/j.1432-0436.1998.00193.x.
[52] E. Rossi, I. Gerges, A. Tocchio, M. Tamplenizza, P. Aprile, C. Recordati, F. Martello, I. Martin, P. Milani, C. Lenardi, Biologically and mechanically driven design of an RGD-mimetic macroporous foam for adipose tissue engineering applications, Biomaterials. 104 (2016) 65–77, https://doi.org/10.1016/j.biomaterials.2016.07.004.
[53] A.L. Berlin, M. Hussain, D.J. Goldberg, Calcium hydroxylapatite filler for facial rejuvenation: a histologic and immunohistochemical analysis, Dermatologic Surg. 34 (2008) S64–S67, https://doi.org/10.1111/j.1524-4725.2008.34245.x.
[54] F. Simunovic, S. Schlager, M. Montanari, N. Iblher, Prospective 3D analysis of facial soft tissue augmentation with calcium hydroxylapatite, J. Cosmet. Laser Ther. 19 (2017) 283–289, https://doi.org/10.1080/14764172.2017.1307411.
[55] D.G. Wallace, H. Reihanian, B.B. Pharriss, W.G. Braun, Injectable implant composition having improved intrudability, 1989.
[56] Ranella J. Hirsch, J.L. Cohen, Soft tissue augmentation, US6432437B1, 2006.